DAMPING EFFECTS IN MEMS RESONATORS

M. Gologanu, C.G. Bostan, V. Avramescu, O. Buiu,

Sensors and Wireless Lab Bucharest (SWLB), ACS Sensors and Wireless Laboratory, Honeywell Romania SRL,
169A Calea Floreasca, Bucharest, Romania
E-mail: mihai.gologanu@honeywell.com

Abstract–*Damping effects are very important in MEMS-based sensors and actuators. In this paper we use analytical models and finite element (FE) computations to quantify the energy losses due to viscous fluid damping, acoustic radiation and thermo-elastic damping. To treat the case where squeeze/slide film models can not be applied, we have implemented in a commercial FE package a new incompressible flow solver based on a gauge formulation. We are thus able to solve for full flows around complex 3D geometries in the frequency domain and predict viscous damping of resonant MEMS structures. The full methodology is exemplified on the response of a MEMS silicon resonator, including acoustic driving and piezoelectric sensing.*

Keywords: *MEMS, Damping, Modelling*

1. INTRODUCTION

MEMS resonators are the main building blocks of many types of new tiny devices used in a wide range of applications, from RF modules to sophisticated inertial sensors. Beyond the challenges imposed by every specific application and design strategy, there is a common parameter of paramount importance for whatever use of the resonators; this is the resonator quality factor (Q) which describes energy damping effects.

From this perspective, the main issue is to understand and quantify all damping effects affecting a vibrating structure; then one needs to engineer the resonator for an increased Q factor leading to better sensitivity of the device/sensor.

This paper presents analytical and COMSOL® FE models for different kinds of damping mechanisms that help the device designer to choose the best suited geometry for a particular application.

The working device chosen for this study is a silicon tuning fork bulk resonator whose shape is presented in Fig. 1. At variance with typical MEMS resonators, we do not intend to use the device in vacuum, but in air at pressures ranging from 0.2bar to atmospheric pressure.

There are some constraints imposed to this resonator by the silicon on insulator (SOI) technology that is intended to be used to build it. It is supposed that the resonator is realised by deep reactive ion etching (DRIE) of a "device" side from a SOI wafer. In order to release the resonator the underneath buried oxide (BOX) must be removed, thus leaving a very narrow gap between the resonator beam and the "handling" side of the SOI wafer (Fig. 1). The dimension of this gap was one of the parameters that our simulation did consider in an extensive manner, in order to evaluate air friction and squeezing effects.

Different silicon walls surround the tines of the tuning fork; the distance between these walls and the tuning fork element were also considered, in order to evaluate the same effects.

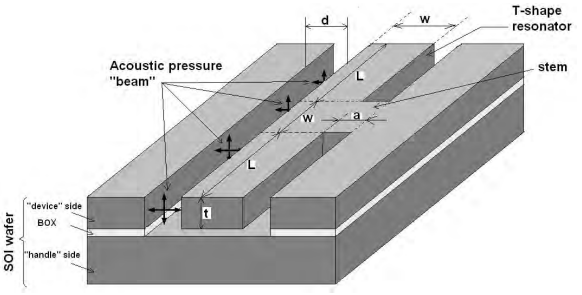

Fig. 1. Planar SOI T-shape resonator.

We assume that the resonator is driven by an acoustic pressure generated by a source that looks like a divergent beam along the tuning fork tines. Each point on this beam will then act as an individual acoustic pressure generator, launching pressure waves that hit the resonator's tines.

The in-plane resonator movement is detected through a 0.5μm thick piezoelectric layer deposited on the top of the silicon tines by sputtering from a ZnO target, as in Fig. 2. The deposition and the patterning of this layer are not discussed here.

There are two strips of piezoelectric layers deposited on each half of the two tines of the

978-1-4673-0738-3/12/$31.00 © 2012 IEEE

resonator, in order to collect the positive and the negatives charges that are generated through the piezoelectric effect when the tines vibrate in the fundamental in-plane bending mode. The generated current is monitored by a transimpedance amplifier that holds the voltage across the piezo layer at zero.

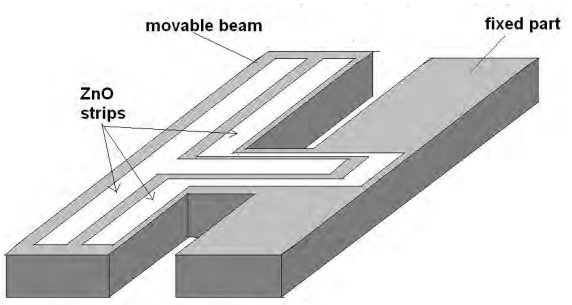

Fig. 2. Configuration of ZnO thin layer("device" side only).

Table 1. Parameters used in the modelling

Item	Notation	Value	Unit
Bean length	L	3	mm
Beam Thickness	t	125	μm
Beam width	w	300	μm
BOX	g	2	μm
Stem length	a	60	μm
Acoustic beam side	d	140	μm
Acoustic source	W_L	$1.6\cdot10^{-4}$	W/m
Initial waist	w_0	6	μm
Waist change	λ	1.5	μm
Sound speed	c	332	m/s
Ambient temperature	T	293.15	K
Viscosity of air	μ	$2\cdot10^{-5}$	Pa·s

Material (anisotropic) parameters for Si and ZnO have been taken from COMSOL material library; isotropic elastic properties for Si, needed for the analytical model, were calculated for the (100) direction.

2. DAMPING MECHANISMS

Damping is a key issue in MEMS based sensors and actuators, being related to energy losses [1, 2]. Quality factor is a quantitative indicator of the energy dissipation, due to overall damping present in the system. The physical definition of Q-factor is:

$$Q = 2\pi \left. \frac{\text{Energy stored}}{\text{Energy dissipated}} \right|_{\text{per cycle}} \qquad (1)$$

Equivalently, the Q-factor can be evaluated from the frequency response, by taking the ratio between the resonant frequency and the -3dB bandwidth (given by the energy dissipation rate).

There are various mechanisms of energy loss and each of them can be considered as an independent term contributing to the overall Q-factor, in a first approximation. Broadly speaking, the damping mechanisms fall into two main categories – fluid and structural:

$$\frac{1}{Q} = \frac{1}{Q_{\text{fluid}}} + \frac{1}{Q_{\text{structural}}} \qquad (2)$$

A supplementary damping mechanism appears here due to acoustic reradiation from the resonator itself.

$$\frac{1}{Q_{\text{fluid}}} = \frac{1}{Q_{\text{viscous}}} + \frac{1}{Q_{radiation}} \qquad (3)$$

Assuming negligible intrinsic material losses, the main categories of structural damping are: thermo-elastic damping (TED) and anchor loss:

$$\frac{1}{Q_{\text{structural}}} = \frac{1}{Q_{\text{TED}}} + \frac{1}{Q_{\text{anchor}}} \qquad (4)$$

The lowest individual Q factor (i.e., largest energy dissipation) dominates the overall Q. In practice, a higher Q means an increased sensitivity and lower power consumption. In this paper we consider the effects of viscous, TED and acoustic radiation on MEMS resonators.

Table 2. Summary of the viscous effects and characteristic numbers showing different regimes of MEMS devices

Effect (number)	Expression	Regimes
Inertial (Reynolds)	$\text{Re} = \frac{\rho_a b^2 \omega}{4\mu}$	Re<<1 - inertial effects are negligible
Compressible (Squeeze)	$\sigma = 12\frac{\mu t^2 \omega}{g^2 p_a}$	σ<<1, compressibility can be neglected
Rarefaction (Knudsen)	$Kn = \frac{\lambda}{h_0}$ $\lambda = p_0\lambda_0 / p_a$	Kn<0.01 continuum flow 0.01<Kn<0.1 slip flow 0.1<Kn<3 transitional Kn>3 molecular flow

ρ_a=gas density; b=characteristic length viscous flow; L= characteristic width of the structure; μ=gas viscosity; p_a=ambient pressure; p_o=101325 Pa ; λ=mean free path of gas molecules; λ_0=64nm mean free path at p_0 and 25^0C; ω=resonance angular frequency.

The parameter λ is related to the local value of the pressure p_a as:

$$\lambda = \frac{p_0 \lambda_0}{p_a} \quad (5)$$

where p_0=101325Pa and λ_0=64nm are the pressure and molecular mean free path for air at t=25^{0}C.

2.1. Squeeze-Film Damping (SFD)

Many dynamic MEMS structures consist in moving plates and beams suspended above a fixed substrate. A thin fluid layer (air or some other gas) is trapped in the gap between the MEMS structure and the substrate. The complex interaction between fluid and vibrating structure results in both damping and stiffening of the structure. When the gap thickness is sufficiently small compared to the lateral dimensions of the structure, the so-called "squeeze-film damping" (SFD) dominates. SFD is affected by various factors: geometry of the structure, oscillation frequency, packaging pressure, thickness of the fluid film, boundary conditions. SFD dominates, often by one or two orders of magnitude over the other damping mechanisms.

The most popular approach in the literature to model SFD effects employs solving Reynolds equation. This equation is deduced for isothermal systems, under the assumption that the gap thickness is much smaller compared to the lateral extent of the plates. In addition, inertia and slip correction factors (thus extending its validity over the entire operating range of MEMS devices) must be included.

A linearized form of the modified Reynolds equation, modelling the frequency response of MEMS, is as follows [3]:

$$\nabla_T \cdot \left(h_0^3 Q_{ch} \nabla_T p_f - 6\mu h_0 \mathbf{u}_T \right) = j\omega 12\mu \left(p_f \frac{h_0}{p_a} + \Delta h \right) \quad (6)$$

where p_f= film pressure in the gap (unknown that is solved for), Q_{ch} = relative flow function, that accounts for inertial and rarefaction effects, Δh=gap deformation (h-h_0), $\mathbf{u_T}$ = tangential velocity of the structure (moving above a fixed substrate). The tangential operator ∇_T refers to the fact that equation is solved on a boundary (x-y plane in the present case).

The different flow regimes that depend on the value of Knudsen number are considered by changing the viscosity term with an effective one (μ_{eff}). Veijola *et al* [4] provided a simple approximation for the effective viscosity:

$$\mu_{eff} = \frac{\mu}{1 + 9.638 \cdot Kn^{1.159}} \quad (7)$$

This was achieved by fitting the flow rate coefficients to the more complicated expression proposed by Fukui and Kaneko [5] which are based on Boltzmann transport equation.

Formula (7) extends the validity of modified Reynolds equation to the range 0<Kn<880 (from continuum to molecular flow), with an accuracy of 5%.

Assuming a gap thickness h_0=10μm and using the definition of Kn from Table 2 and the equation (5), one gets the minimum packaging pressure for which approximation (6) is still valid:

$$p_a^{\min} = \frac{p_0 \lambda_0}{h_0 Kn^{\max}} \cong 0.737 \text{ Pa} \quad (8)$$

When the resonance frequency and the gap thickness are high enough (10's of kHz and 10's of μm, respectively), inertial effects become important and the relative flow function becomes a function of frequency. Veijola [6] provided a low-frequency, first-order approximation for Q_{ch}. Including the gas inertial and rarefaction effects, the expression for Q_{ch} to be used in equation (6) is:

$$Q_{ch} = \frac{1 + 9.638 Kn^{1.159}}{1 + j\omega \dfrac{\rho h^2 \left(1 + 10Kn + 30Kn^2\right)}{10\mu \left(1 + 9.638 Kn^{1.159}\right)}} \quad (9)$$

Expressions correcting for the end effects (supplementary pressure drop at the margin of the plate) have also been proposed in the literature–they consist in artificially increasing the dimensions of the plate with a length proportional to the gap.

2.2. Gauge Finite Element Method for Harmonic Hncompressible Viscous Flows

Faced with this bewildering choice of squeeze film models based on various approaches, approximations and limitations, a MEMS designer would greatly benefit from a full flow simulation around the entire vibrating structure, at least as a mean to check various assumptions underlying the SFD models. The first difficulty is that all Navier-Stokes numerical solvers that we are aware of do not propose a harmonic solver. The second difficulty is the high computational cost of 3D flow simulations around a complex MEMS structure. At variance with the wide-held belief that such flow

simulations are not practical, we will show that the use of the gauge finite element method (as proposed by E and Liu [7] and closely related to the impulse formulation of the Navier-Stokes equations) will permit us to obtain by direct harmonic simulation the damping of a complex structure. Due to space constraints, we will discuss here only the incompressible case.

The Navier-Stokes equations are given by:

$$\rho\frac{\partial u}{\partial t}+(u\cdot\nabla)u=-\nabla p+\mu\Delta u;\ \nabla\cdot u=0 \qquad (10)$$

where u is the velocity, p the pressure, ρ the density and μ the dynamic viscosity of the fluid. Assuming that the amplitude of vibration is small, we can then neglect the nonlinear convection term; assuming further harmonic expressions for velocity and pressure: $u=u\exp(j\omega t),\ p=p\exp(j\omega t)$, one obtains:

$$j\omega\rho u=-\nabla p+\mu\Delta u;\quad \nabla\cdot u=0 \qquad (11)$$

Following E and Liu [7] we now introduce auxiliary variables a and φ (gauge variable) by:

$$u=a+\nabla\varphi \qquad (12)$$

When introduced in the previous equations, we obtain the following system of equations:

$$\Delta a=j\omega a;\qquad \Delta\varphi=-\nabla\cdot a \qquad (13)$$

and the pressure can be determined after solving for the auxiliary variables by:

$$p=\mu\Delta\varphi-j\omega\rho\varphi \qquad (14)$$

The advantage of this gauge formulation is that we can fix arbitrary the gauge φ by choosing freely the boundary conditions for it, contrary to other numerical implementation where the determination of correct boundary conditions for some auxiliary variables (like pressure for projection methods or vorticity for stream-vorticity methods) poses big problems. E and Liu [7] have proposed to use either Dirichlet or Neumann boundary conditions for the gauge variable; our numerical tests have shown an advantage for the latter:

$$\frac{\partial\varphi}{\partial n}=0;\ \ a\cdot n=u_b\cdot n;\ \ a\cdot\tau+\frac{\partial\varphi}{\partial\tau}=u_b\cdot\tau \qquad (15)$$

This condition is applied on a boundary where the velocity $u=u_b$ is imposed with n the boundary normal and $\tau=\tau_1,\tau=\tau_2$ the boundary tangential directions.

In practice, one has to solve the system (15) of elliptic equations, coupled only at the boundary or through volume terms. One can use an iterative strategy, where one solves in turn each equation separately (and where one can accelerate the overall convergence by using the extrapolation strategy for the gauge variable as proposed in E and Liu [7]) or directly the coupled system.

Once the solution is found, the total force acting on a body of with boundary S can be readily determined from:

$$F=\int_S\left(j\omega\rho\varphi n+\mu\frac{\partial a}{\partial n}\right)dS \qquad (16)$$

The merit of this expression lies in the use of precisely those terms that are determined with higher precision in a finite element solution (like for example the normal derivative at a boundary of a primary variable). Similar expressions have been found for the total moment acting on rigid body and also for the total mechanical work done by fluid forces on a flexible vibrating structure.

The gauge method has been implemented in COMSOL® and validated using a series of simple problems with analytical solutions. We note that slip conditions typical for rarefied flows with Knudsen number 0.01<Kn<0.1 are also easily implemented in the gauge formulation; on the contrary compressibility effects pose a much more difficult challenge and will be discussed elsewhere.

2.3 Thermo-Elastic Damping (TED)

Thermo-elastic damping (TED) is a source of intrinsic damping in MEMS, driven by the coupling between thermo-elasticity and elasto-dynamics. When a cyclic stress is applied to a structure, it leads to an oscillatory deformation. Some parts of the structure will be compressed (and heated-up) while other parts will be stretched (and cooled-down). These induced temperature gradients will generate a heat flow and an irreversible loss of energy. A characteristic time scale of this phenomenon is the thermal relaxation time constant - the effective time that the material requires to relax after an applied constant stress or strain. When the vibration frequency is close to the thermal relaxation frequency, the TED dissipation effect is most pronounced.

The coupled equation of heat conduction in terms of normal strains is:

$$\nabla(\kappa\nabla T) = \rho C_p \frac{\partial T}{\partial t} + \frac{E\alpha T_0}{1-2\nu}\cdot\frac{\partial(\varepsilon_x+\varepsilon_y+\varepsilon_z)}{\partial t} \qquad (17)$$

where ρ = material density, C_p = heat capacity at constant pressure, κ = thermal conduction, α = thermal expansion coefficient, ε_i = normal strains, E = Young's modulus, ν= Poisson's ratio, T_0 =nominal equilibrium temperature (ambient). Consider a harmonic variation of temperature $T = \tilde{T}e^{j\omega t}$, where $j\omega = -\lambda$ is the complex angular frequency. Then, the heat conduction equation can be expressed as:

$$-\nabla(\kappa\nabla\tilde{T}) = -j\omega(\rho C_p\tilde{T} + T_0 S_{elast}) \qquad (18)$$

where the right-hand side is the heat-source term and S_{elast} is the elastic entropy per unit volume.

2.4. Other Losses

When a mechanical element moves it can generate sound waves that will lead to another potential damping mechanism-*acoustic radiation*.

There are two distinct regimes for acoustic radiation, characterized by mechanical frequencies either smaller or larger than the "coincidence" frequency. At this frequency, the characteristic wavelength of the mechanical structure becomes comparable to the wavelength of pressure waves, and this marks the onset of strong acoustic radiation, with high energy losses that may dominate other damping mechanisms. Many vibrating MEMS structures operate well below the coincidence frequency, where acoustic damping is generally negligible compared to other damping mechanisms. However, operation at higher modes at ultrasonic frequencies will approach coincidence.

Support losses arise from resultant shear forces and moments at the end supports, which transfer energy from the vibrating element to the substrate, by exciting elastic waves; these waves carry part of the vibration energy that will be dissipated into the substrate. For example, the resonator (Fig.1) is clamped to the lateral wall by a stem. The resonator is symmetric and vibrates in a balanced way without moving its center of mass. In this case, the shear forces and moments cancel and the support (stem) losses are minimized.

3. ACOUSTIC PRESSURE DRIVE

As discussed In each plane perpendicular to the generating beam, we suppose that the source is Gaussian; the waist of this Gaussian increases along the generating beam but the total acoustic energy transferred in each plane is a constant W_L.

The acoustic harmonic drive of the device is modelled by the following equation in cylindrical coordinates centered on the acoustic beam axis:

$$j\omega^2 p + c^2\Delta p = j\omega\frac{2W_L}{\pi w(z)^2}\exp\frac{-2r^2}{w(z)^2} \qquad (19)$$

where W_L=1.65×10^{-4} W/m represents the total acoustic power in each plane perpendicular on the z axis and w the waist that is given by:

$$w(z) = w_0\left[1+\left(\lambda z/\pi w_0^2\right)^2\right]^{1/2} \qquad (20)$$

4. ANALYTICAL MODEL

When operated in an open environment with no walls and substrate effects, our device is amenable to a full analytical solution; because of space constraints we present here only the main steps. Radiation damping will be neglected in the present analytical model.

Petra *et al.* [8] have provided an analytical solution for the acoustic pressure generated by a constant waist beam in infinite space. In our case, the waist varies only slowly with z, and their solution can be used in each plane perpendicular to the acoustic beam axis:

$$p(r,z) = \frac{W_L}{\omega w(z)^2}\left[h(\infty)J_0(s) - j\left(g(s)J_0(s)+h(s)Y_0(s)\right)\right]$$

where J_0 and Y_0 are Bessel functions, $s = \omega r/c$ and:

$$g(s) = \int_s^\infty tY_0(t)\exp\frac{-2t^2c}{\omega w(z)^2}dt,\ h(s) = \int_0^s tJ_0(t)\exp\frac{-2t^2c}{\omega w(z)^2}dt$$

The free vibrations of each tine can be modelled by a clamped-free beam with the first eigenmode given by:

$$\Phi(x) = ch(ax) - c(ax) + \left(s(ax) - sh(ax)\right)\frac{ch(a)+c(a)}{sh(a)+s(a)}$$

where x is the position along the beam normalized by the length L, *c,s,ch,sh* are the trigonometric and hyperbolic cos and sin functions and a solves 1+c(a)ch(a)=0, while the corresponding eigenfrequency is given by:

$$\omega_0 = \frac{a^2}{L^2}\sqrt{\frac{EI}{\rho A}}$$

where E is Young modulus, A, I are cross-section area and moment of inertia and ρ is the solid density.

When the free modes are well separated and damping is small, one can solve the damped vibrations around a mode by supposing that the beam movement is proportional to the eigenmode Φ with an unknown amplitude A. Using the weak formulation of the structural equations with test function equal to the complex conjugate of Φ, one easily obtains:

$$A(\omega) = \frac{\int f_{drive}\overline{\Phi}}{\left(\omega_0^2 - \omega^2\right)\int \rho\Phi\overline{\Phi} - \int f_{damp}\overline{\Phi}}$$

where the integrals represent the mechanical work done by drive or damping forces and the kinetic energy respectively. Noting

$$G = \frac{\int f_{damp}\overline{\Phi}}{\omega_0^2 \int \rho\Phi\overline{\Phi}} = G_r + jG_i \qquad (21)$$

the normalized mechanical work of the damping forces, one can follow Sader [9] to show that the amplitude $|A(\omega)|$ dependence is similar to that of a standard resonator if one defines the resonance frequency ω_r and quality factor Q by:

$$\omega_r^2 = \omega_0^2 \frac{1}{1+G_r}, \qquad Q = \frac{G_r + 1}{G_i} \qquad (22)$$

For a beam vibrating in an open viscous gas, one can use the methodology proposed by Sader [9] to estimate the viscous damping. One supposes that the flow around the beam at a certain position along the beam is well approximated by the flow around a *rigid* beam of the same section having a harmonic displacement equal to that of the original beam at the said position. One can show that in general, the hydrodynamic loading force is:

$$F_{hydro} = \frac{\pi}{4}\rho_a \omega^2 b^2 \Gamma(\omega) U$$

where b is the nominal width of the beam section, U is the amplitude of the movement perpendicular to the beam axis and $\Gamma(\omega)$ is a dimensionless "hydrodynamic function". For a beam with circular cross-section of diameter b, the analytical solution is well-known [9]:

$$\Gamma_{cyl}(\omega) = 1 + \frac{4jK_1(-j\sqrt{j\mathrm{Re}})}{\sqrt{j\mathrm{Re}}K_0(\sqrt{j\mathrm{Re}})}, \qquad \mathrm{Re} = \frac{\rho_a \omega b^2}{4\mu}$$

where K_0,K_1 are modified Bessel functions. In our case, the beam has a rectangular cross-section with width T; we approximate it with a cylinder with diameter $b=1.4T$.

Thermoelastic damping for a clamped-free beam has been analytically evaluated by Lifshitz and Roukes [10]:

$$\frac{1}{Q} = \frac{E\alpha^2 T_0}{C_p}\frac{6}{\xi^2}\left(1 - \frac{\sin\xi + \sinh\xi}{\xi(\cos\xi + \cosh\xi)}\right), \xi = t\sqrt{\frac{\omega_0 C_p}{2\kappa}}$$

where α is the thermal expansion coefficient, κ the thermal conductivity and C_p the volumetric heat capacity.

Because the eigen-mode is known, we can easily calculate the strains at the top surface of the beam, transform them to surface charge density ρ_e (using conditions of zero voltage on top and bottom surfaces of the ZnO layer) and calculate the generated current and the effective piezoelectric coupling constant:

$$I = \omega\int \rho_e dA \qquad \beta = I / \Phi(1)$$

The above equations have been implemented in Octave. The theoretical eigenfrequency was 36.6kHz. The theoretical Q-factor for thernoelastic damping was 142000 and will be further neglected; the effective piezoelectric coupling constant was 18μC/m (including both tines). We also obtained the following viscous damping and mass loading in open air:

Table 3. Analytical model results

Pressure [atm]	Quality Factor	Frequency shift [Hz]	Current [pA]
1	10734	-7.9	107
0.5	15428	-4.3	153
0.2	23771	-1.9	238

5. FE SIMULATIONS

The FE results have been obtained by using COMSOL® Multiphysics, a widely used commercial package that implements the finite element discretization scheme. We applied it for the following problems:

(1) Undamped eigenmodes and piezoelectric sensing
(2) Acoustic pressure generation and drive
(3) Acoustic re-radiation
(4) 2D hydrodynamic function using the gauge solver
(5) Viscous damping using SFD and 3D gauge solver
(6) Thermoelastic damping

Solving the eigenfrequencies of the undamped system provided the target values around which the complex eigenfrequencies of the damped system were searched for. The

complex eigenvalue $\lambda = -j\omega$ of a damped system contains information about both the resonant eigenfrequency and the Q-factor:

$$\omega_r = |\operatorname{Im}\lambda|, \qquad Q = \left|\frac{\operatorname{Im}(\lambda)}{2\operatorname{Re}(\lambda)}\right|$$

In cases where this method was not feasible in COMSOL (like the gauge solver), we used the method described for the analytical model and based on expression (21-22).

5.1. Undamped Modes and Piezo Sensing

The un-damped eigenmodes are purely piezo-mechanical, neglecting any other potential interactions. All the boundary conditions were set "free", except the bottom face of the Si wafer that was "fixed".

Fig. 3. Top-view of driving/sensing mode at 37658 Hz; also shown the surface charge density on top of the ZnO layer.

The symmetrical in-plane bending mode (see Fig. 3) has a frequency of 37.7kHz and a total piezoelectric coupling constant of 15.1μC/m, smaller than the theoretical value of 18μC/m (this is due to the fact that ZnO layers do not reach the margins of the tines, where strains are the largest). The unsymmetrical mode is at 30.2kHz and has zero coupling constant. Changing the stem length does alter this last frequency, but does not affect the symmetric mode. This provides a design mean to effectively separate the two modes, valid also at lower Q factors.

5.2. Acoustic Pressure Drive and Re-Radiation

To model acoustic pressure drive and re-radiation, we have modelled the air around the device; silicon walls were considered as hard sound boundaries. The top was considered open and modelled as a half cylinder with radiation boundaries eliminating the reflection of acous-tic outgoing waves. The same approach can be applied to package that replaces the open top.

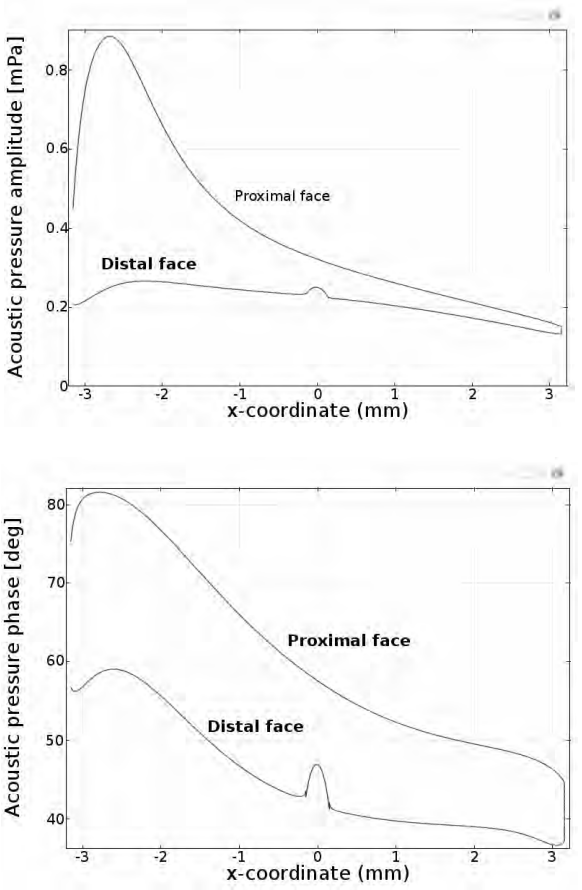

Fig. 4. Amplitude and phase of acoustic drive pressure along the tines - upper curve corresponds to the tine's boundaries facing the acoustic beam, lower curve to the distant ones.

Fig.4 shows the amplitude and phase of the acoustic pressure along the tine lateral faces. The pressure difference between the top and bottom curves in Fig. 4 is the actually driver of the resonator; the small phase difference will slightly change this pressure difference. It is also clear that an improved design will position the acoustic pressure source such that the maximal pressure acts on the tine tip. Because the waist of the acoustic source increases strongly with distance along the tines, the pressure drive is almost zero at the other tine tip; a collimated acoustic source will probably increase the driving force. The lateral wall and the substrate enhance the acoustic pressure by reflecting back acoustic waves. For example, the acoustic pressure close to the substrate is 50% larger than that close to the top face.

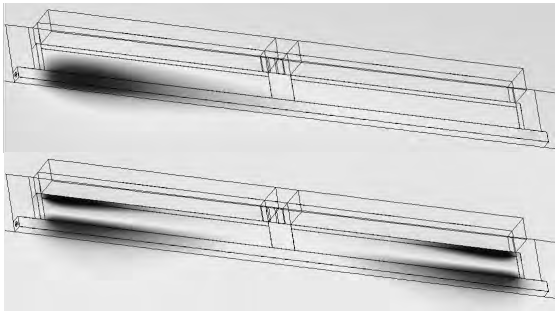

Fig. 5. Acoustic pressure drive (top) and radiation (bottom).

To model acoustic re-radiation we need to couple the structural and acoustic physics– acoustic pressure acts on the tine boundaries while the tine normal accelerations are acoustic sources. We have used the damped eigenvalue solution corresponding to the structural free mode and obtained a radiation Q factor of 858752 and a frequency shift of -9Hz. Fig. 5 shows the difference between acoustic drive and re-radiation at the resonant frequency–while in the first case only one tine tip is practically driven by the acoustic pressure, in the second case both tine tips contribute equally to the re-radiation, each being equivalent to a dipole source. In the sequel we will neglect the acoustic radiation damping.

5.3. Viscous Damping Using 2D Gauge Solver

Passing now to the viscous damping, we first consider some 2D flow simulations that can strongly improve the predictions of the analytical model. Indeed, the most drastic approximation was to replace the rectangular cross-section of the real device with a circular one, in order to use some analytical expression of the hydrodynamic function. For the case of a ribbon, Sader has used earlier results obtained by Tuck [11] and presented them under the form of a fitted correction function that multiplies the circular hydrodynamic function. Actually, the same solution could be applied to an arbitrary cross-section but the methodology is rather complex– one needs to solve an integral equation posed on the cross-section boundary, equation obtained by Tuck [11] with the help of the vorticity-potential formulation of incompressible harmonic flow.

We propose a much simpler solution that uses the 2D gauge formulation to solve numerically for the flow around an arbitrary cross-section. Fig. 6 shows the real and imaginary parts of the hydrodynamic functions obtained for the cylinder, ribbon and rectangle, all with the same characteristic length of 125μm. The analytical result for the cylinder is not included, as it is virtually the same as the numerical one (relative errors around 0.1%). It appears clearly that both the mass loading and viscous damping are much larger for our rectangle than for both cylinder and ribbon.

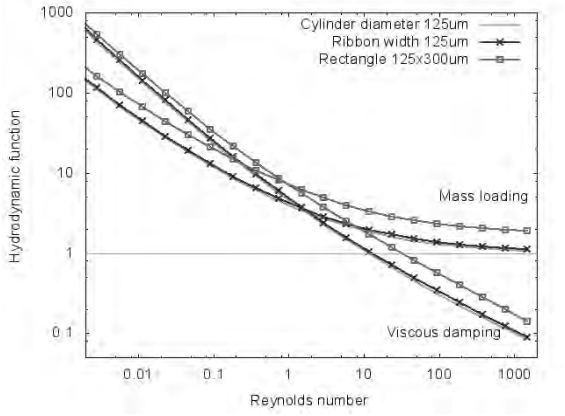

Fig. 6. Hydrodynamic functions for several cross-sections, obtained using the gauge harmonic solver. Reynolds number was varied by changing the frequency.

But we can do much better – we can actually include the surrounding walls, gaps, etc., as shown in Fig. 7, to obtain the "best" hydrodynamic function to be used with the analytical model. It appears that while the 2μm gap respects as expected all suppositions of a slide film model, the flow in the lateral gaps is far from that predicted by squeeze film model. Indeed, the pressure should be constant across the film, while Fig. 7 shows that is not at all true. Also, shear deformation on the top will add to the friction, and will become comparable to the gap friction when the gap is increased to large values.

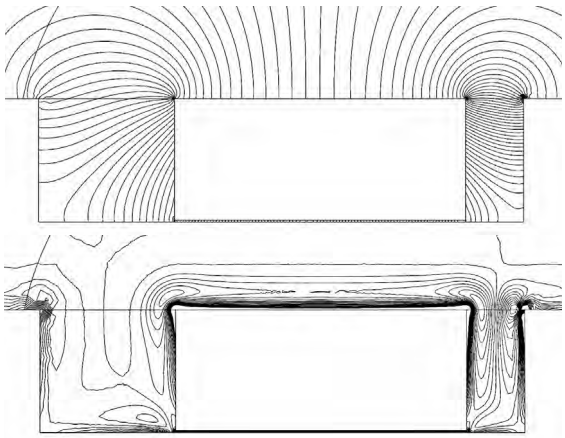

Fig. 7. Flow around a tine section vibrating horizontally, obtained with the 2D gauge solver. The gap and lateral walls are included. Top: pressure; bottom: shear rate.

5.4. Squeeze-Film and 3D Viscous Damping

We next consider the full 3D structure. It is rather easy to include squeeze/slide film damping, using the pre-defined COMSOL® mode "Solid Stress-Strain with Film Damping" with a frequency response analysis, in which the frequency was derived from the eigenvalue. Full Reynolds model equation (6) with flow rate expression (9) was implemented. The bottom of the tines experiences slide film damping in the gap, while the lateral faces experience squeeze film damping. The limits of SFD models appear when we increase the substrate gap – it is then unclear what edge condition to apply for the squeeze film on the lateral faces. Indeed, for small gaps, the substrate acts as a wall and the entire fluid must enter/exit through the top, as seen in Fig. 7. For large gaps, the bottom edge becomes an open one while for intermediate values, gas will escape through the gap itself and this is difficult to model.

Fig. 8. Flow simulation using 3D gauge solver. Top: shear rate in the gap; bottom: pressure on the lateral face.

We have therefore run a full 3D simulation for the harmonic flow of air around the entire structure. Fig.8 shows that end effects are important both in the gap and the lateral face, with damping forces decreasing close to the tip with maximal displacement – these effects are missing in both the 2D hydrodynamic function and the SFD models.

5.5. Thermoelastic Damping

The damped eigenmodes due to TED have been calculated by coupling the thermal and structural physics. A damped eigenfrequency analysis provides a Q-factor of 127674, less than the theoretical value of 142000 (see a possible explanation in [12]). Still, TED can be neglected compared to viscous damping.

5.6. FE Results

Table 4 shows the Q-factors for viscous damping models. It appears that even for this simple geometry, SFD overestimates the Q-factor; the analytical model combined with FE evaluation of the hydrodynamic function is closer to the full 3D simulation. If the entire substrate is removed beneath the tuning fork, then the total Q-factor combining all damping mechanisms is 4520 giving a current of 40 pA at atmospheric pressure.

Table 4. FE model results

Design	3D Flow	Analytical + 2D	SFD
2 μm gap	2204	2911	5819
5 μm gap	2841	3821	11014
9 μm gap	2913	4188	14916
100 μm gap	3672	5438	28342
300 um gap	4687	7642	N/A
Free	5515	7996	N/A

6. CONCLUSIONS AND FURTHER DEVELOPMENT

Damping effects are important in MEMS based sensors and actuators. Energy loss mechanisms like radiation, viscous and thermoelastic damping in complex structures can be well handled in 3D FEM in different regimes, including corrections for rarefaction, inertial and slip-boundary effects. At variance with the wide-held belief that full flow simulation for a complex MEMS structure are not practical, we have shown that the use of the gauge finite element method (implemented in COMSOL®) permits the full 3D modelling of real structure.

References

[1] R. Pratap, S. Mohite, A. K. Pandey, "Squeeze Film Effects in MEMS Devices", *Journal of the Indian Institute of Science*, **87**(1), pp. 75–94.

[2] M. Bao, H. Yang, Y. Suna, Y. Wang, "Squeeze-film air damping of thick hole-plate", *Sens. Actuat. A* **108**, pp. 212–217, 2003.

[3] A.K. Pandey, R. Pratap, F.S. Chau, "Influence of Boundary Conditions on the Dynamic Characteristics of Squeeze Films in MEMS Devices", *J. Microel. Syst*., **16**(4), pp. 893–903, 2007.

[4] T. Veijola, H. Kuisma, J. Lahdenperä, T. Ryhänen, "Equivalent-circuit model of the squeezed gas film in a silicon accelerometer", *Sens. Actuat. A*, **48**, pp. 239–248, 1995.

[5] S. Fukui, R. Kaneko, "Analysis of ultra-thin gas film lubrication based on linearized Boltzman equation: first report- derivation of a generalized lubrication equation including thermal creep flow", *Trans. ASME J. Tribol.*, **110**(2), pp. 253–262, 1988.

[6] T. Veijola, "Compact models for squeezed-film dampers with inertial and rarefied gas effects", *J. Micromech. Microeng*, **14**, pp. 1109–1118, 2004.

[7] W.E, J-G Liu, “Gauge finite element method for incompressible flows”, I*nt. J. Numer. Meth. Fluids*, **34**, pp. 701–710, 2000.

[8] N. Petra, J. Zweck, A.A. Kosterev, S. E. Minkoff, D. Thomazy, “Theoretical analysis of a quartz-enhanced photoacoustic spectroscopy sensor”, *App. Phys. B*, **94(**4), pp. 673–680, 2009.

[9] J.E. Sader, “Frequency response of cantilever beams immersed in viscous fluids with applications to the atomic force microscope”, *J. Appl. Phys*., **84**(1), pp. 64–76, 1998.

[10] R. Lifschitz, M.L. Roukes, “Thermoelastic Damping in Micro/Nanomechanical Systems”, *Phys. Rev. B*, **61**, pp. 5600–9.

[11] E.O. Tuck, Calculation of unsteady flows due to small motions of cylinders in a viscous fluid, *J. Eng. Math.*, **3**, pp. 29–44, 1969.

[12] A. Duwel, R.N. Candler, T.W. Kenny, M. Varghese, “Engineering MEMS resonators with low thermoelastic damping”, *J. MEMS*, **15**(6), pp. 1437–1445, 2006.